Available online at www.sciencedirect.com
SCIENCE DIRECT®
Journal of Nuclear Materials 347 (2005) 266–288
journal of nuclear materials
www.elsevier.com/locate/jnucmat

Chamber wall materials response to pulsed ions at power-plant level fluences ☆,☆☆

T.J. Renk [a,*], P.P. Provencio [a], T.J. Tanaka [a], C.L. Olson [a], R.R. Peterson [b], J.E. Stolp [c], D.G. Schroen [c], T.R. Knowles [d]

[a] *Sandia National Laboratories, MS 1193, P.O. Box 5800, Albuquerque, NM 87185-1193, United States*
[b] *Los Alamos National Laboratory, NM, United States*
[c] *Schafer Corp., Livermore, CA, United States*
[d] *Energy Science Laboratories, Inc., San Diego, CA, United States*

Abstract

Candidate dry-wall materials for the reactor chambers of future laser-driven Inertial Fusion Energy (IFE) power plants have been exposed to ion pulses from RHEPP-1, located at Sandia National Laboratories. These pulses simulate the MeV-level ion pulses with fluences of up to 20 J/cm^2 that can be expected to impinge on the first wall of such future plants. Various forms of tungsten and tungsten alloy were subjected to up to 1600 pulses, usually while being heated to 600 °C. Other metals were exposed as well. Thresholds for roughening and material removal, and evolution of surface morphology were measured and compared with code predictions for materials response. Powder-metallurgy (PM) tungsten is observed to undergo surface roughening and subsurface crack formation that evolves over hundreds of pulses, and which can occur both below and above the melt threshold. This roughening is worse than for other metals, and worse than for either tungsten alloyed with rhenium (W25Re), or for CVD and single-crystal forms of tungsten. Carbon, particularly the form used in composite material, appears to suffer material loss well below its sublimation point. Some engineered materials were also investigated. It appears that some modification to PM tungsten is required for its successful use in a reactor environment.

1. Introduction

The first wall of an Inertial Fusion Energy (IFE) power plant will be subjected to intense pulsed neutrons, X-rays, and energetic ions produced from explosions of fusion material at the reactor chamber center. An experimental investigation is underway at Sandia National Laboratories of the effects of these ion and X-ray pulses on candidate chamber dry-wall materials. The energetic ions are produced by the RHEPP-1 facility, and the X-rays by the *Z*

☆ Sandia is a multiprogram laboratory operated by Sandia Corporation, a Lockheed-Martin Company, for the United States Department of Energy under Contract DE-AC04-94AL84000.
☆☆ Supported by NRL through the HAPL Program by the US Department of Energy, NNSA, DP.
* Corresponding author. Tel.: +1 505 845 7491; fax: +1 505 845 7864.
E-mail address: tjrenk@sandia.gov (T.J. Renk).

0022-3115/$ - see front matter © 2005 Elsevier B.V. All rights reserved.
doi:10.1016/j.jnucmat.2005.08.021

facility. Materials exposure results from Z are discussed elsewhere in this issue. We report here on the exposure of first-wall armor materials to intense ion beams. The RHEPP-1 (Repetitive High Energy Pulsed Power) accelerator was used to produce fluences of either helium or nitrogen ions of up to 10 J/cm^2 per pulse, with ion energies as high as 1.8 MeV (for doubly charged nitrogen). The repetitive capability of RHEPP-1 resulted in sample exposure to many ion pulses, as many as 1600 per sample investigated. The ion current pulsewidth varied from 150 ns to nearly 500 ns. As discussed in the paper by Sethian et al. in this issue, this time is shorter than the debris ion arrival time, but comparable to the fusion product arrival time expected in future reactors. Accordingly, the fluence thresholds discussed below may be lower than what might be expected for an actual reactor, as the diffusion into the substrate occurring with longer pulsed energy delivery times mitigates the surface heating effect.

A future laser IFE reactor may be operated at a pulse rate as high as 10 Hz. This amounts to an annual total of 3×10^8 pulses to the first wall. Besides the considerable thermal energy delivered to the wall surface on each pulse, there likely will be effects of a thermomechanical nature caused by the pulsed energy delivery, such as expansion of the near-surface region against the (relatively) unheated subsurface, fatigue responses, etc. Ions with up to 20 J/cm^2 fluences and several MeV energies will impinge normal to and penetrate well below the surface (1–10 μm). Surface sputtering can be secondary to ablation/sublimation of the wall surface. To ensure survivability, effectively no erosion of the flat wall surface per pulse can be tolerated (<1 nm/pulse). In addition to high melting/vaporization points, additional durability can be expected from materials with good ductility, fatigue response, and high thermal conductivity. 'Engineered' materials, e.g. with non-flat geometry, may also be constructed in a way to better distribute the heat load and mechanical stresses.

Initially, the investigative emphasis was on determining the threshold for both surface ablation, and surface roughening, as shown in Fig. 1. Sample exposure consisted of multiple single-pulse events, on the order of 50 or 75. For example, the roughening threshold measured for powder-metallurgy tungsten (PM W) [1] at room temperature (RT) was determined by monitoring the reflected light from an initially smooth surface with a laser reflectometer at increasing fluence per pulse. Using the

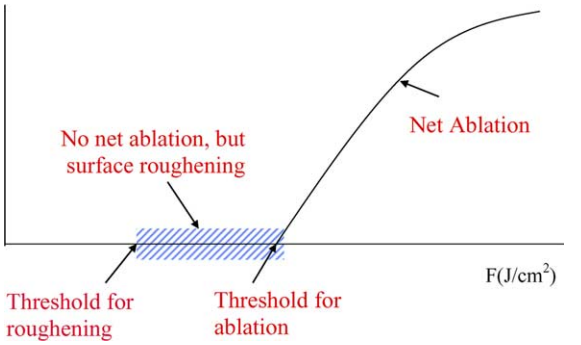

Fig. 1. Schematic of plan for investigation of surface roughening and ablation.

nitrogen beam from RHEPP-1, the received signal was observed to remain constant until a level of 1.25 J/cm^2 was reached. At this level, each subsequent pulse produced a progressive reduction in received signal from the previous pulse. This indicates that the laser light was increasingly scattered by the roughening surface. The total number of pulses in this case was 53. In another experiment, the ablation threshold for unheated PM W was determined to be about 6 J/cm^2, by monitoring the step height produced at the boundary of exposed and unexposed surface, using a 1-D profilometer. This value is consistent with predictions from both the BUCKY [2] and SIM [3] modeling codes.

The next step then was to determine if the exposed sample would remain unaffected by repeated exposures below the measured thresholds. The number of exposures was greatly increased [4]. It was found that for unheated PM W exposed to 400 pulses (nitrogen), an exposure below the 1.25 J/cm^2 fluence threshold resulted in no increase to surface roughness, whereas above this value, the level of roughening (measured by the roughness parameter R_a) increased dramatically with beam fluence. For other materials, such as the carbon matrix portion of carbon fiber composite (CFC), it is unclear whether there is a lower fluence limit below which the sample remains unaffected (see discussion below). More significantly, however, it became clear from such studies that the materials response to large numbers of ion pulses can become quite complex, and can take hundreds of pulses to evolve. The effects appear to have various causes, such as thermomechanical and fatigue response in the case of PM W, or possibly physical sputtering or radiation-enhanced sublimation in the case of the CFC matrix material.

We discuss here the results of such long-term exposures, with the focus primarily on tungsten in various forms, tungsten alloys, and graphite in the form of CFC. In addition, several other metals were investigated for surface response, to compare with these materials. The other metals include molybdenum, titanium, and copper. The tungsten was usually heated to 600 °C, a temperature which is above its ductile-brittle transition temperature (DBTT). Some other elements were also exposed at this temperature, depending upon the space available in a given exposure series.

To survive in a fusion reactor, the chamber wall surface must remain free from material loss over many pulses. The most obvious source of material loss is surface sublimation due to the surface temperature exceeding the material vaporization threshold. This can be avoided by restricting the surface temperature excursion. Physical sputtering is another source of material loss, and is more prevalent in low-Z materials such as graphite. Surface roughening is a concern inasmuch as it can lead to a mechanically unstable surface morphology, e.g. large peak-to-valley excursions, which may be accompanied by cracking which propagates below the surface. If the surface evolution were to reach a saturation point, this might be tolerable provided the mechanism for saturation is understood and determined to be benign. However, if the surface undergoes exfoliation, for example, the shed material may result in the surface roughness reaching a plateau value, but shedding of course means material loss that will eventually compromise the wall surface. The leading dry-wall candidate material is a tungsten coating on ferritic steel. If crack propagation initiates in the tungsten, accompanied by surface exfoliation, the cracks may eventually reach the underlying steel support material, and could cause failure of the chamber wall.

So it is important to understand the causes, thermal and thermomechanical, of the roughening mechanism that is seen in short-term exposures of treated materials, in order to make conclusions about long term survival in a power plant. Surface roughening can be affected by a number of mechanisms, including alloying with volatile elements such as sulphur, the presence of entrained gases, and the material grain size and microstructure. Surface morphology evolution can thus be expected to be a function of grain size and near-surface microstructure, as will be seen in the discussion of PM, single-crystal, and CVD forms of tungsten below. Roughening can also differ, for the same fluence, depending upon the ion composition of the beam.

2. Experimental setup and test procedure

Flat-geometry samples of various metals, including pure tungsten (W) formed by both powder metallurgy and CVD were prepared, along with single-crystal W. To compare with the performance of pure W, flat samples of W–25Re (25% Rhenium) were also prepared. This alloy is used in applications such as thermocouple wiring, where increased ductility is desired. The W–25Re melting point is about 400 K less than that for pure W (3680 K). In addition to the flat samples, several examples of non-flat or 'engineered' materials were investigated. Graphite in the form of 'velvet', i.e. long fibers oriented parallel to the flux direction, was coated with a sputtered layer of 1.6 μm-thick W, and exposed to ion doses. Also, a three-dimensional 'foam' material [5] consisting of a complex of 'bridges' was investigated.

After exposure to the RHEPP-1 beam, measurements of surface roughening and ablation were made with one- and two-dimensional profilometry. Estimates of overall mass loss were made by masking off part of the sample, and then comparing surface profiles across the treatment interface. Effects on surface topology and near-surface microstructure were studied using secondary electron microscopy (SEM) and cross-sectional transmission electron microscopy (XTEM). Surface composition was studied with energy dispersive spectrometry (EDS). In the discussions below, these results are compared with predictions of materials response from the BUCKY and SIM modeling codes. BUCKY is a one-dimensional Lagrangian radiation hydrodynamics computer code. The code includes time and energy-dependent deposition of multiple ion species with multiple charge states. The code calculates heat transfer in materials via thermal diffusion and multi-group radiation diffusion to produce time-dependent temperature profiles in a material irradiated with RHEPP ions. Temperature-dependent thermal properties are used in the thermal diffusion calculation. The heat of fusion is included in the temperature-dependent heat capacity and the properties of molten tungsten are used above the melting temperature [6]. SIM is a much simpler code that contains energy deposition using the TRIM [7] code, with the measured ion beam current density near the sample, in addition to the

corrected voltage of the ion emission as propagated to the sample location. This is similar to the BUCKY energy input process. Bulk properties similar to those in BUCKY are also input. Since only 1-D heat diffusion is considered, without hydrodynamic effects or vaporization, the code gives rapid turn-around response predictions, and aids in determining the positioning of samples within the beam for exposure.

The (RHEPP-1) ion beam facility has been described elsewhere [8,9]. The beam is formed in the MAP (Magnetically confined Anode Plasma) ion diode. For this work, beams were formed from either nitrogen ($45\%N^{2+}/45\%N^{1+}/10\%H$) or helium ($\sim 100\%He^{1+}$). The He pulse may better simulate the effect of the fusion products arrival, and features a longer pulsewidth than N (approaching 0.5 μs compared to 200–300 ns). Fluence is limited to about 3 J/cm^2 compared to the 8 J/cm^2 possible with N. Diode voltage varied from 600 to 900 kV over the 100 ns power pulse with nitrogen, and was somewhat lower with He (~500–600 kV). The diode-sample distance was typically 40 cm. Current densities varied, depending upon sample location, from 200 A/cm^2 peak to less than 20 A/cm^2 over a 150 cm^2 total area. Nearby charge collectors monitored the ion beam fluence as a function of sample location. The ions penetrate several microns into the test material, and induce a rapid heating, followed by rapid cooling (10^9 K/s) as the thermal pulse diffuses into the substrate. At high enough fluences, sublimation/ablation of the surface occurs. In the multi-shot exposure series, the time between pulses is about 15 s, and samples which were originally at room temperature can become quite hot to the touch afterwards. In the case where the samples are heated to 600 °C, thermocouple readings confirm that this temperature is held throughout the exposure series.

Each pulse delivers roughly a monolayer of ions ($\sim 10^{14}$/cm^2) at depths up to ~1 μm, so that compositional changes in the treated material due to the added ions can be said to be minor. With 1000 pulse exposures, some effects due to ion implantation might be possible, although a sample of W exposed to 1000 nitrogen pulses and examined with XTEM showed no signs of gas accumulation. In the case of helium, other researchers have reported bubble formation in He-implanted test samples, but at implanted doses significantly higher than what would be entrained here as a result of the 450 He pulse series described below.

3. Ion beam exposure experiments

The discussion below is divided into the general categories of materials discussed above, i.e. (a) tungsten and tungsten alloy, (b) other metals, (c) carbon composite, and (d) engineered surfaces.

3.1. Tungsten and tungsten–25%Re alloy

Tungsten is the focus of interest both for inertial fusion energy (IFE) and magnetic fusion energy (MFE) research in first-wall materials. This is due to its high melting point and mechanical durability. However, tungsten is also known to be quite brittle. It is apparently this brittleness which is the cause of the materials response to ions discussed here. Of all the metals investigated, the PM form of tungsten exhibits the most pronounced tendency to roughen. In some cases, the differences between W and other metals is striking. As mentioned above, the mere fact of roughening may not be significant for long-term reactor survival if it can be shown that (1) the roughening reaches a saturation point, (2) no net material loss is observed, and (3) any fatigue cracking does not propagate to the substrate beneath.

The roughening threshold for PM W was previously measured at 1.25 J/cm^2 using the RHEPP-1 N beam. The sample (unheated) was exposed to over 50 pulses during this measurement. A SIM heat-flow simulation of pure W response to a 1.25 J/cm^2 N beam predicts a peak surface temperature of about 1800 K. A BUCKY simulation of tungsten was performed using the RHEPP-1 nitrogen beam with a fluence of 1 J/cm^2. The predicted temperature, yield stress and thermal stress at the surface of the tungsten are shown in Fig. 2 at $t = 152$ ns, where the tungsten is initially at room temperature. BUCKY does not currently have an internal material strength model. Thermal stresses and temperature-dependent yield stresses [10] are calculated via post-processing of BUCKY-produced temperature profiles. At about $t = 80$ ns the surface temperature begins to rapidly rise as the main ion beam pulse arrives, so the thermal stress at the surface also begins to rise, while the yield stress on the surface falls. At about $t = 100$ ns, the surface thermal stress becomes larger than the yield stress, and plastic flow could begin to occur. At $t = 152$ ns, the surface temperature and surface stress reach maxima. In Fig. 2, the temperature, thermal stress and yield stress are all plotted versus distance from

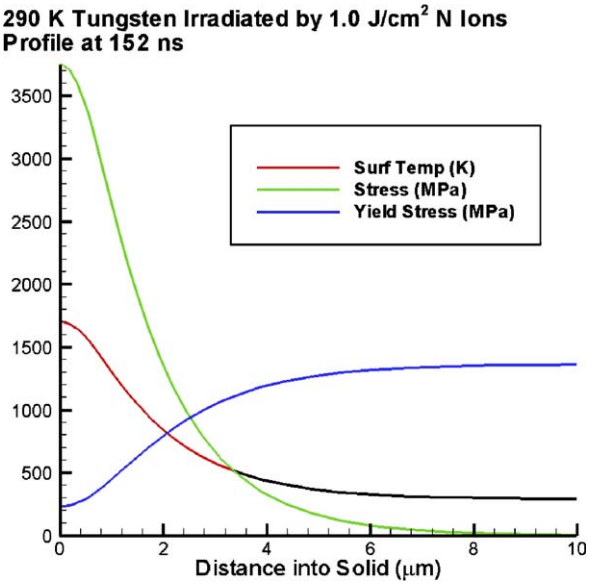

Fig. 2. Surface temperature, surface stress, and surface yield stress versus distance from surface at 152 ns for room temperature tungsten irradiated with 1.0 J/cm^2 of nitrogen ions on RHEPP.

the surface at $t = 152$ ns. At distances as much as 2.5 μm below the surface, the thermal stress is greater than yield stress, and plastic flow may be present. This will roughen that material, so these BUCKY calculations predict that there may be surface roughening at a RHEPP-1 nitrogen beam fluence of 1 J/cm^2. The BUCKY predicted surface temperature at 1 J/cm^2 is 1700 K, which is consistent with the SIM estimate. A BUCKY simulation at as low as 0.5 J/cm^2 still shows some yielding.

Both the SIM and BUCKY predictions for surface temperature are well below the tungsten melting temperature of 3680 K. The BUCKY prediction of surface yielding at or even below 1 J/cm^2 is less than the experimentally measured 1.25 J/cm^2. This may be due to either local uncertainty in fluence determination, and/or a sensitivity effect with the laser reflectometer. In any case, it appears that thermomechanical response of the tungsten is the cause of the roughening. In addition to the possibility of yield and plastic flow, the near-surface layer will expand and then cool after the ion pulse, whereas the substrate does not. The surface can be expected to remain in a distorted state, compared to before the pulse. The effects can be expected to accumulate with repeated exposure.

To determine the response of a PM W surface to ion beam exposure above and below the 1.25 J/cm^2 threshold, a polished and unheated sample was subjected to 400 pulses of the MAP N beam, over a fluence range per pulse between 1 and 3.7 J/cm^2 [4]. Surface roughness (R_a) measured with 1-D profilometry did not increase above the untreated level below the threshold level. Above this value, however, the R_a rapidly increased with dose, reaching over 20 μm at 3.7 J/cm^2 fluence, with peak-to-valley (P–V) surface excursions exceeding 70 μm.

To further study the evolution of surface relief with both number of exposures and fluence level, a series of multi-pulse exposures was performed: (1) a 600-pulse series with various metal samples, including PM W and PM Mo heated to 600 °C and treated with the MAP nitrogen beam at an average per-pulse fluence of 4.5 J/cm^2 – melting conditions; (2) a 1000 pulse series similar to (1), where the PM W and PM Mo were treated at 2.5 J/cm^2 – at or slightly above melting; (3) a 450-pulse series with PMW, CVD W, and single-crystal W, heated to 600 °C and treated with the MAP He beam at a low fluence level of 1–1.3 J/cm^2. This last fluence level was chosen to be at or below the roughening threshold measured for the nitrogen beam. In the case of (1) and (2), the samples were heated and exposed to 200 pulses at a time, then were demounted and checked for surface roughness by 1-D profilometry (DekTak). They were then re-mounted in the same relative positions and exposed to another 200 pulses, until the series was completed. In the case of the He series, the samples were subjected to the entire 450 pulses, after which both DekTak measurements and SEM imaging was performed.

An example of the surface morphology after treatment can be seen in Fig. 3. The figure shows an SEM image (160× magnification) of a portion of the surface of the single-crystal W after 450 He pulses, including the treatment interface at top. Visible in the image are a series of cracks, with possible valleys as well as raised areas. (Both are seen in the DekTak scans.) The cracks tend to be vertically oriented, presumably following crystallographic planes. In the case of the PM W material, the cracks tend to be randomly oriented, as are the grains. These cracks are evidently initiated due to surface fatigue, because they become evident after hundreds of pulses. (Micro-cracking with negligible surface height is visible almost immediately with exposure.)

A comprehensive summary of the DekTak data for the various tungsten forms is presented in Fig. 4. Results of peak–valley measurements from

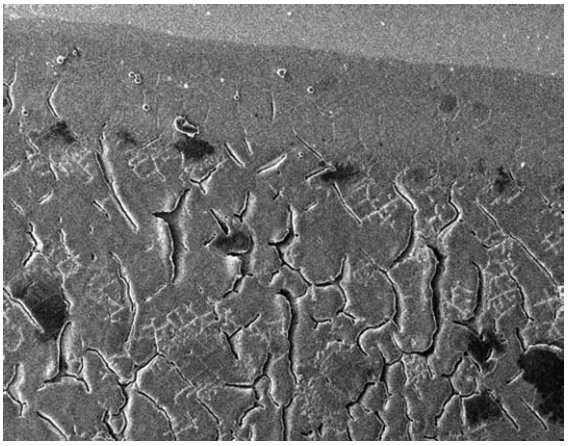

Fig. 3. SEM Image of Single-crystal W, showing interface between treated (450 pulses, He Beam) area (below) and untreated (above) areas. Treatment fluence 1–1.3 J/cm^2, sample heated to 600 °C.

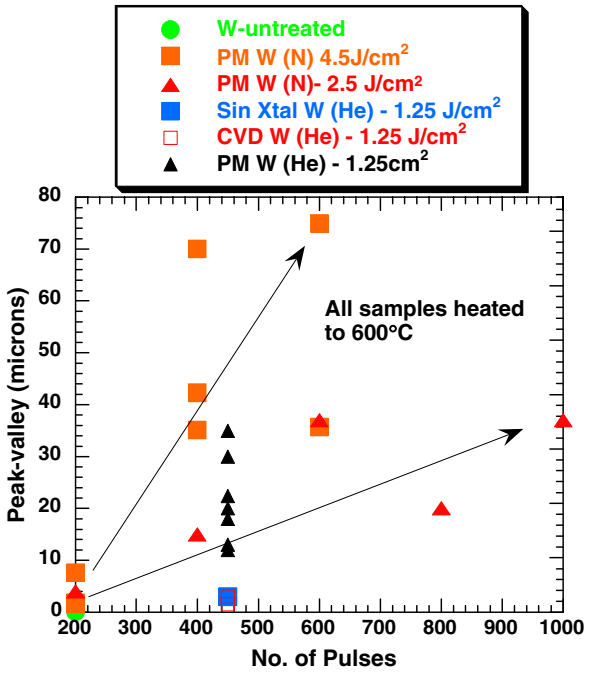

Fig. 4. Evolution of peak–valley excursions for PM W as a function of number of MAP N ion pulses. Fluence is 2.5 J/cm^2 for 1000 pulses, and 4.5 J for 600 pulses. Also shown are P–V values for PM W, CVD W, and single-crystal W for 450 pulses of MAP He beam at 1–1.3 J/cm^2.

all three series listed above are shown. A plot of the surface parameter R_a shows almost identical behavior. The PM W 2.5 J/cm^2 and 4.5 J/cm^2 measurements are taken every 200 pulses, whereas the He data are measured only at the end of the 450-pulse series. Several trends are noticeable: (1) the P–V evolution is roughly linear in the number of MAP N pulses; (2) the P–V surface excursions increase at roughly twice the rate at 4.5 J/cm^2, compared to 2.5 J/cm^2; (3) very little surface relief develops until after the first 200 pulses; (4) the P–V roughening of PM W with He is relatively worse than for nitrogen. The roughening with He at 1–1.3 J/cm^2 for 450 pulses is worse than for the same number of pulses of nitrogen, even when the latter are at 2.5 J/cm^2 per pulse; and (5) the roughening of PM W is significantly worse than for CVD W and single-crystal W at the same fluence and number of pulses (He). Item 4 is consistent with previous measurements [10] which show that heavier ions produce smoother surface topology, despite the fact that their shallower penetration leads to higher peak surface temperatures for the same beam fluence. Evidently, the roughening threshold is lower than 1.25 J/cm^2 when He ions are used.

The most notable result from these measurements is that PM W exhibits the strongest propensity to roughen, whether helium or nitrogen ions are used as the treatment ion. The PM W roughening, besides being worse than for the other W forms, is also much worse than for either the heated PM Mo sample, or the unheated W25Re, pure Re, commercially pure Ti, and copper samples that were also exposed. This is indicated in Fig. 5, which shows the evolution of the surface roughness parameter R_a for the following (flat) materials: PM W, W25Re, pure Re, pure Mo, Ti-2 (commercially pure), Al 1100, and Cu. The 2.5 J/cm^2 fluence is high enough to melt the metals listed, and in the case of Al 1100, this fluence produces near-vaporization of the surface, which may account for the high R_a values for the Al. The roughness values for PM W, although quite high, indicate a possible saturation condition after about 600 pulses. The W25Re and Re roughness remains well below the R_a values for PM W, reaching about 1 μm after 1000 pulses. The values for PM Mo and Ti-2, although also remaining well below the PM W values, show a tendency to increase without saturation till the end of the series. Note also that the roughness of Cu shows no real change from the untreated values over 800 pulses. A similar plot of data taken at 4 J/cm^2 looks almost identical, but with the y-axis values doubled in magnitude.

Further BUCKY calculations were performed, to show the scaling of the tungsten response with ion species (nitrogen or helium beams) and fluence

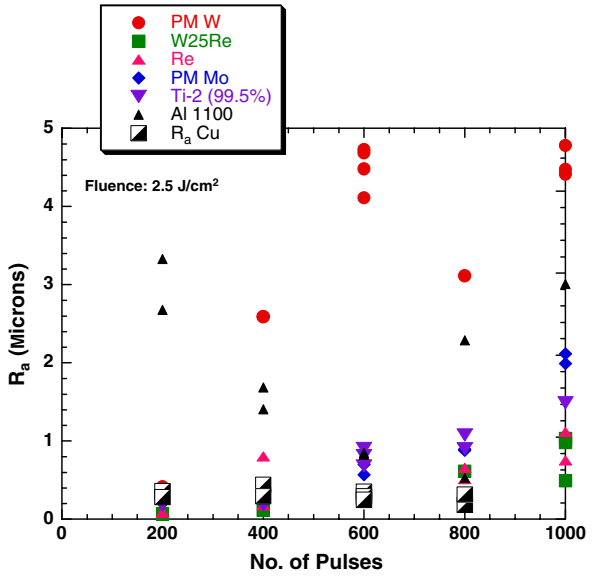

Fig. 5. Evolution of R_a for a number of materials as a function of number of MAP N ion pulses. Fluence is 2.5 J/cm^2 for 1000 pulses. The PM W and PM Mo were heated to 600 °C. The W25Re, Re, Ti-2, Al 1100, and Cu were initially at room temperature.

variation. The W surface temperature was set initially to either room temperature (RT), or 600 °C (873 K). The scaling of peak surface temperature with fluence is shown in Fig. 6 for the four cases (nitrogen beam, or He beam, RT and 873 K initial temp). Melt depth scaling is plotted in Fig. 7. As can be seen, melt depth and surface temperature

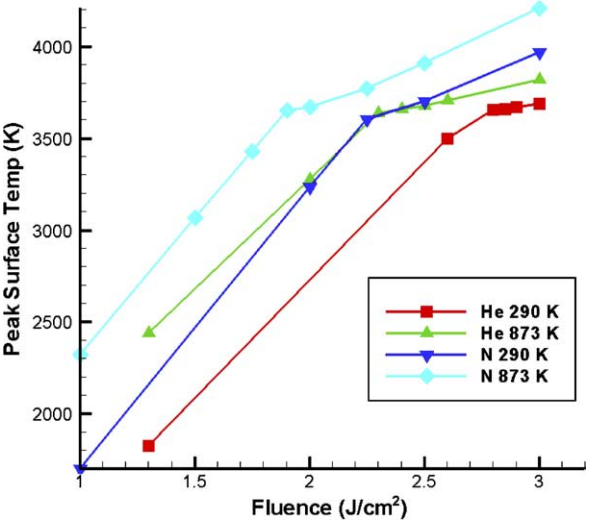

Fig. 6. Maximum surface temperature of heated and un-heated tungsten irradiated with RHEPP helium and nitrogen beams.

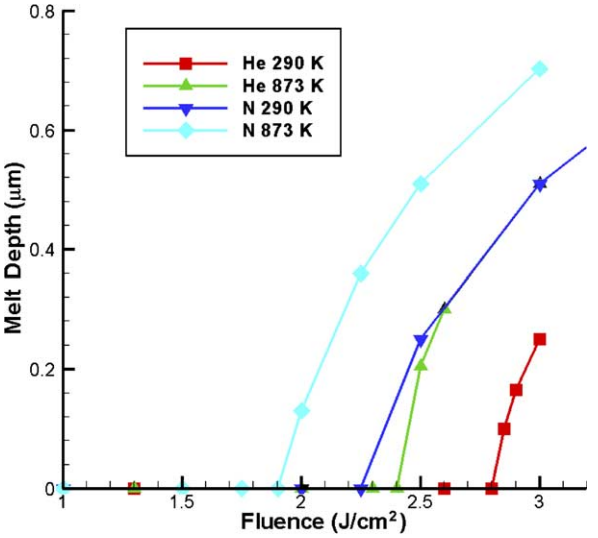

Fig. 7. Melt depth of heated and un-heated tungsten irradiated with RHEPP helium and nitrogen beams.

are highest for the heated W surface irradiated with nitrogen ions. This is due to the shallower penetration of nitrogen compared to helium, which concentrates the deposited energy closer to the surface. Note also that the slope of the peak temperature curve is reduced when the material begins to melt. The thresholds for melting and peak surface temperatures at a fluence of 3 J/cm^2 are shown in Table 1. It should be pointed out that the various treatment series discussed here have occurred at slightly different treatment distances, so that the parameters shown in Table 1 and Figs. 6 and 7 may vary with each series.

It is important to determine if the roughening seen here will reach a saturation point or not. This requires some insight into the mechanism of the roughening process. Fatigue cracking has already been alluded to above. Since the roughening develops over hundreds of pulses, some form of fatigue or work hardening of the surface would appear to

Table 1
BUCKY predictions of thresholds for melting and peak surface temperature at 3 J/cm^2 for tungsten irradiated with RHEPP ions

Ion species	Initial temperature (K)	Melt threshold (J/cm^2)	Peak surface temperature at 3 J/cm^2 (K)
N	290	2.25	3970
N	873	1.9	4211
He	290	2.4	3497
He	873	2.8	3820

play a key role. Another sample set was prepared, and treated by the MAP nitrogen beam over a total of 1600 pulses. The fluence per pulse varied between 1.2 and 1.7 J/cm^2 for the set as a whole, i.e. lower than the exposures discussed above, but for more pulses. The sample set consisted of flat samples, in addition to several kinds of 'foam', i.e. engineered surface [5]. The foam will be discussed separately below. The flat samples consisted of PM W, W25Re, and Ti-2. After every 400 pulses, SEM images were taken of the treated surfaces. Halfway through the series, a second W25Re sample was included, so that surface data were available for 1600 and 800 pulses of the same material at the same time.

The result of the SEM observations for treated PM W are shown in Fig. 8(a)–(d), where surfaces are shown for 400, 800, 1200 and 1600 pulses, respectively. The PM W was heated to 600 °C for all pulses, and the magnification shown is 2000×. The estimated per-pulse fluence was 1.5 J/cm^2. Heat-flow SIM simulations indicate that the peak surface temperature reached about 3000 K, i.e. below the melting point for W. Conjecture about morphology evolution seen in SEM images is of course qualitative, since depth information can be ambiguous. In the first image at 400 pulses (Fig. 8(a)), a network of cracks is observed to form, leading to a set of 'pad-like' structures, each about 10–20 μm in extent. These cracks are observed to follow some grain boundaries, but then may cross these boundaries as well. Along the cracks, features form which look like exfoliation structures. As the number of pulses increases, these structures increase in number and extent, and eventually 'join up' to form valley-like features (Fig. 8(c)). Some rounded

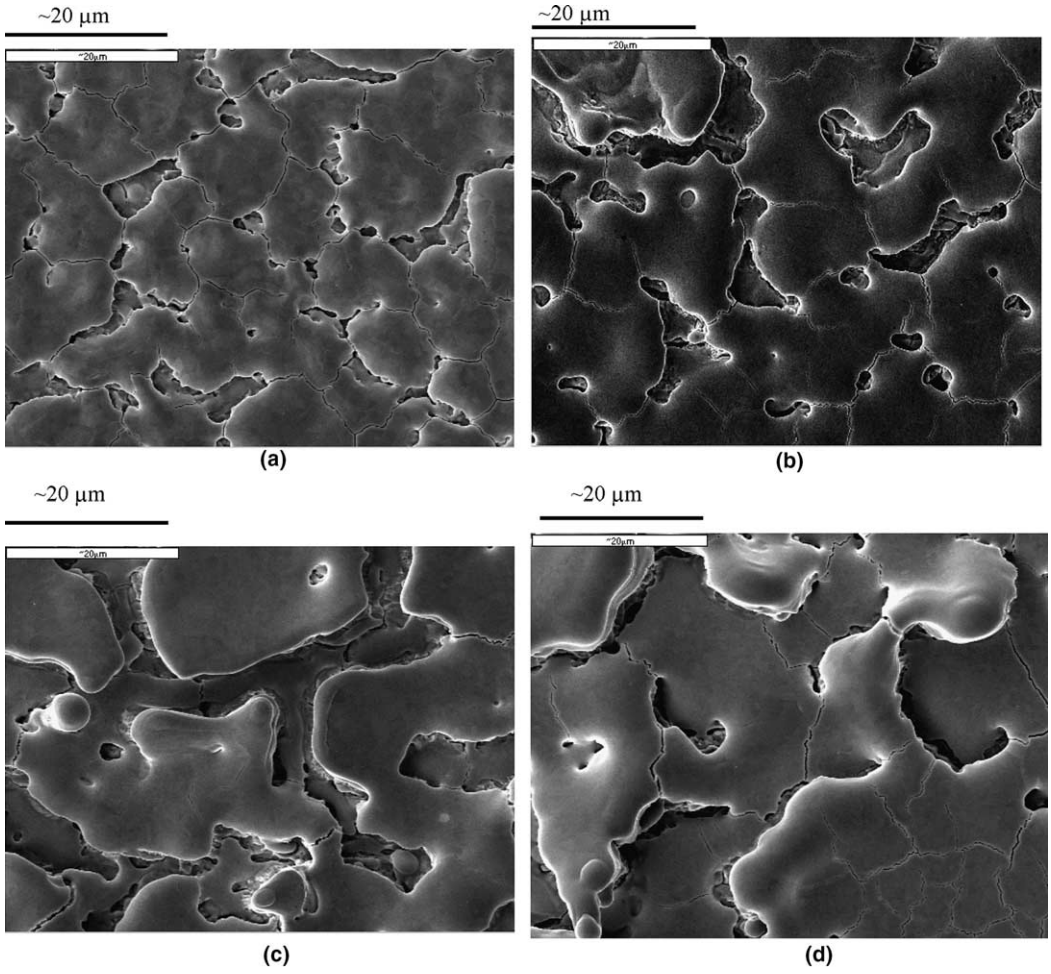

Fig. 8. SEM images of PM W taken after 400 (a), 800 (b), 1200 (c), and 1600 (d) nitrogen pulses. Fluence is approximately 1.5 J/cm^2.

knobs are also visible, and these appear to be in a higher position than the valleys. Although EDS analysis of some of these knobs indicate the presence of Cu particles brought to the surface from the beam generation area, the majority of the knobs analyzed are verified as W in content. The image at 1600 pulses (Fig. 8(d)) appears to show the most complex topology, with features appearing to be both above and below some reference height.

These general features – cracking pattern followed by 'valley' formation in a general pad-like pattern, are repeated in the other metals subjected to ion beam exposure, with the exception of copper, which develops no relief, even after 800 pulses. This is presumably due to the ductile properties of Cu.

The two features in particular mentioned above – exfoliation appearance and 'valley' formation, are important as indicators of possible mass loss in the treated surface. If either could be confirmed, this could lead to the conclusion of unacceptable mass loss. In the case of these experiments, no weighing of samples before/after was undertaken, which would be the most direct way to confirm mass loss by exfoliation. Such a measurement may be compromised anyway by the observation of added Cu to the surface during treatment, originating in the beam generation process.

The issue of 'valley' formation, however, can be addressed by the determination of the overall surface height of the treated region, compared to a reference. The reference in these experiments is the untreated zone, so measurements have been made across the treatment interface. The samples have been mechanically smoothed prior to treatment to establish a flat region that could be so referenced.

An adjoining area of the PM W surface, mentioned above, that was treated with 450 He pulses at 1–1.3 J/cm^2, was later subjected to 600 pulses of the MAP N beam at 4 J/cm^2. A small zone in between these two regions was kept as an untreated reference. Dektak profilometer measurements were made of the He-treated area after 450 pulses, and then of the nitrogen-treated area, after 200, 400, and 600 pulses. Profiles of three scans are shown in Fig. 9(a)–(c). On the left side is the scan, with the R_a and P–V values for the PM W after 450 He pulses (1–3 and 10–30 μm, respectively). On the right side are the corresponding numbers for MAP N treatment after 200 pulses (a), 400 pulses (b), and 600 pulses (c). The untreated zone is in between, at approximately 2000–4000 μm (horizontal position).

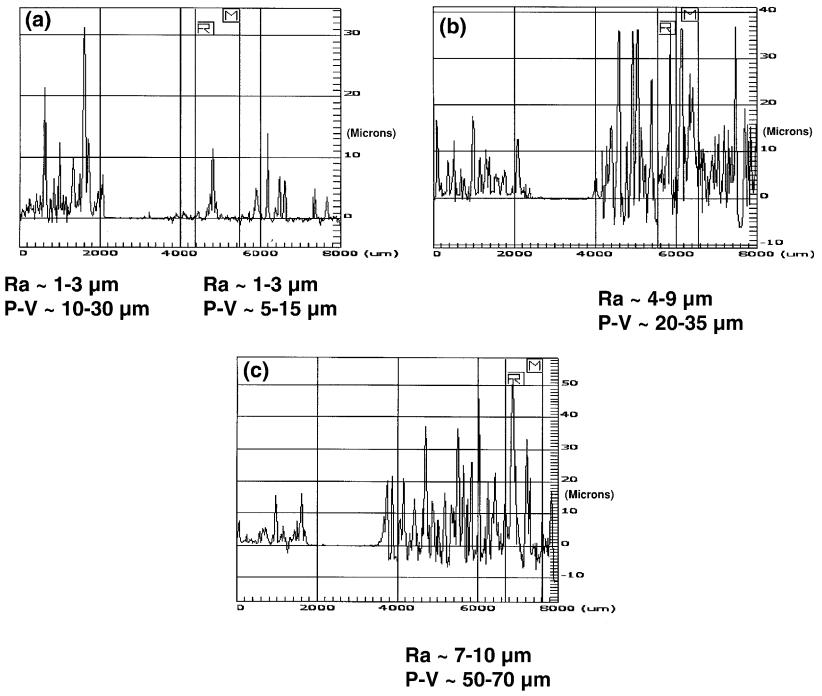

Fig. 9. 1-D Dektak scan profiles of PM W. Left side is after 450 pulses He beam in all cases, the right side is after nitrogen beam pulses of 200 (a), 400 (b), and 600 (c) in number. The R_a and P–V values for each surface are noted.

The left side features appear to diminish from (a) to (c), but that is only because the vertical axis scale is increased to account for the increased roughness of the N-treated side from 200 to 600 pulses.

There are two notable features to point out here: (1) the R_a and P–V values are observed to increase steadily with pulse number, reaching 7–10 μm and 50–70 μm, respectively. This roughness exceeds that seen on the He side both because of the higher per-pulse fluence, and because of the larger number of total pulses. It should be noted that the 4 J/cm^2 fluence on W renders the surface temperature well above melt. (2) Relative to the (middle) untreated zone, the overall height of the treated surface tends to *increase*, rather than decrease. The level of 'valley' depth is slightly higher at 600 pulses compared to 400, but in either case, the minimum height, relative to the untreated zone, is less than 10 μm, whereas the 'mountains' can reach 60 μm in height.

The determination of absolute height is verified by laser profilometry of the treated W surface after 1600 pulses. A comprehensive surface map of most of the treated area is shown, along with the untreated area along the outside, in Fig. 10. This map was made by a NEXIV Laser Profilometer (Nikon Model VMR-3020). This plot clearly shows a general increase in height of the treated surface.

These observations taken together lead to the following tentative conclusions about the roughening: two possible sources of mass loss – exfoliation, and valley formation, have been identified. It is outside the scope of these experiments to verify that the apparent exfoliation, which looks evident in the SEM images, is really taking place, and really leading to mass loss. However, the 'valley' formation scenario looks to be more of a 'mountain' formation scenario. Presumably, the source of the mountain-building relief may be the expansion of the surface due to thermal heating while the substrate remains relatively unexpanded. If the relief is mostly due to mountains, as it appears, then overall there may be a redistribution of surface mass, but not compelling evidence of outright mass loss, at least in these experiments.

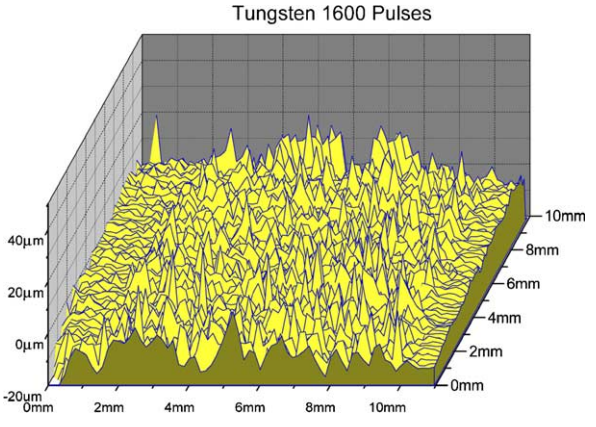

Fig. 10. Comprehensive scan using NEXIV Laser Interferometer of treated PM W, 1600 pulses at an average 1.5 J/cm^2.

A survey of the SEM images, as well as images produced by two-dimensional VEECO analysis of prior treated samples, indicates that the cracks seen tend to reach significant depths. The VEECO images show a network of fine cracks whose width is too narrow to be detected by the Dektak. If it can be shown that these cracks propagate in depth and may reach the underlying substrate, then this could be a predictor of first-wall failure. Stress crack propagation was investigated with the PM W sample subjected to 1000 pulses at an estimated average per-pulse fluence of 2.25 J/cm^2. SIM predicts a peak surface temperature of just over the melting point (3750 K), with a minimal melt depth of 0.1–0.2 μm at most. A portion of the near-surface was removed by the Focused Ion Beam (FIB) technique, and then analyzed by both XTEM and scanning TEM (STEM).

A STEM image of the near-surface region of the treated PM W is shown in Fig. 11. There is no melting or recrystallization evident, either near the surface (a) or at depth (b). Grain morphology looks identical both near the surface and at the 10 μm maximum depth of the FIB cut. Surface roughness reached 2.3–4.5 μm on this sample. Two XTEM images are shown in Fig. 12(a) and (b), with Fig. 12(a) the near-surface region, and Fig. 12(b) at a depth of 5–10 μm. While no melt layer is evident, in both images there are cracks and voids in both the horizontal and vertical directions, and extending the entire distance of the FIB cut. The presumed cause is fatigue cracking.

Compared to the PM W surface, the W25Re exhibits the same qualitative features as the number of nitrogen pulses is increased, but at a more attenuated level. Fig. 13(a)–(c) shows SEM images of W25Re treated under the same conditions as the PM W whose images are shown in Fig. 8, i.e. treatment by nitrogen beam at about 1.5 J/cm^2. Images were taken after 400 (a), 800 (b), and 1200 (c) pulses (an image for 1600 pulses is not available). The measured R_a is much lower than for the PM W sample,

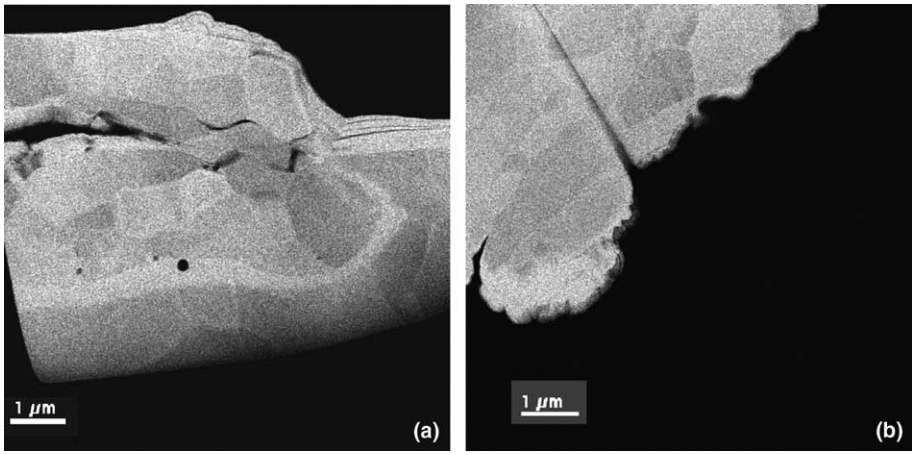

Fig. 11. (a) STEM image of sectioned PM W (heated to 600 °C) treated with 1000 nitrogen pulses at an average fluence per pulse of 2.25 J/cm^2. View near the surface. (b) STEM, same as (a), but at 5–10 μm depth.

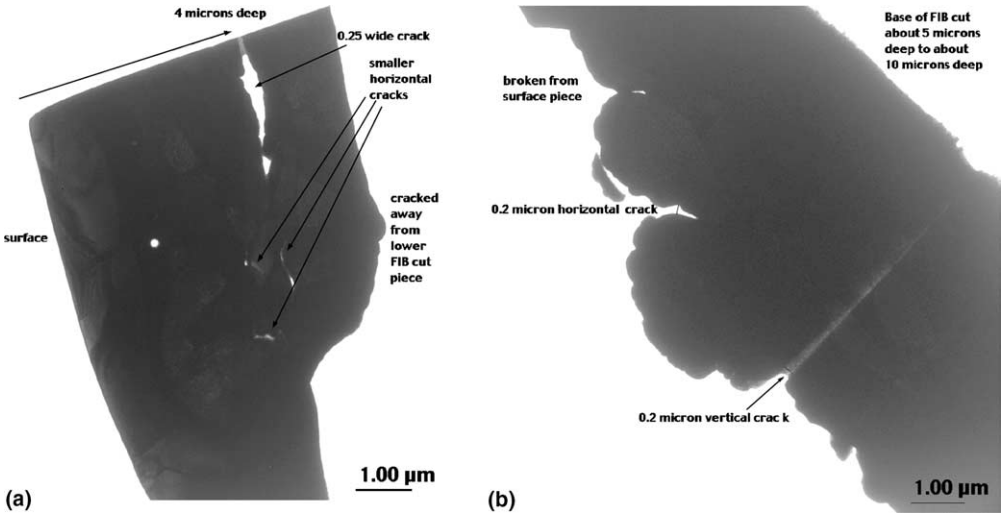

Fig. 12. XTEM images of same sample as Fig. 11, near the surface (a) and at 5–10 μm depth (b).

about 0.6 μm instead of the 2–3 μm level seen with the PM W. It should be noted that, due to the slightly higher fluence used for the W25Re, and its 400 K lower melting point compared to pure W, that the surface of the W25Re probably melted compared to the W which most likely did not melt. Indeed, the W25Re surface shows a clearly shiny appearance compared to the more dull-looking PM W surface. However, this trend of lessened roughening of the W25Re has been clearly established in a number of treatment series. Also, as noted above, the PM W surface showed severe roughening at 4 J/cm^2. This is a treatment level that most certainly produced surface melting of the PM W.

Some exposure of the tungsten was undertaken at high fluence (60 and 400 pulses in two series), enough to ablate the surface (6 J/cm^2 and above). The trend of increased roughening with number of pulses is still evident, although the absolute amount of roughening is reduced. This may be because the melt distances are large enough to smooth out surface perturbations before they build up. Fig. 14(a) and (b) show bright-field XTEM images of a PM W sample that was exposed to 60 nitrogen pulses at an average fluence of 6 J/cm^2. This is the ablation threshold for W. The near-surface region (Fig. 14(a)) shows an epitaxial melt-recrystallization layer of almost 3 μm depth. The surface is smooth

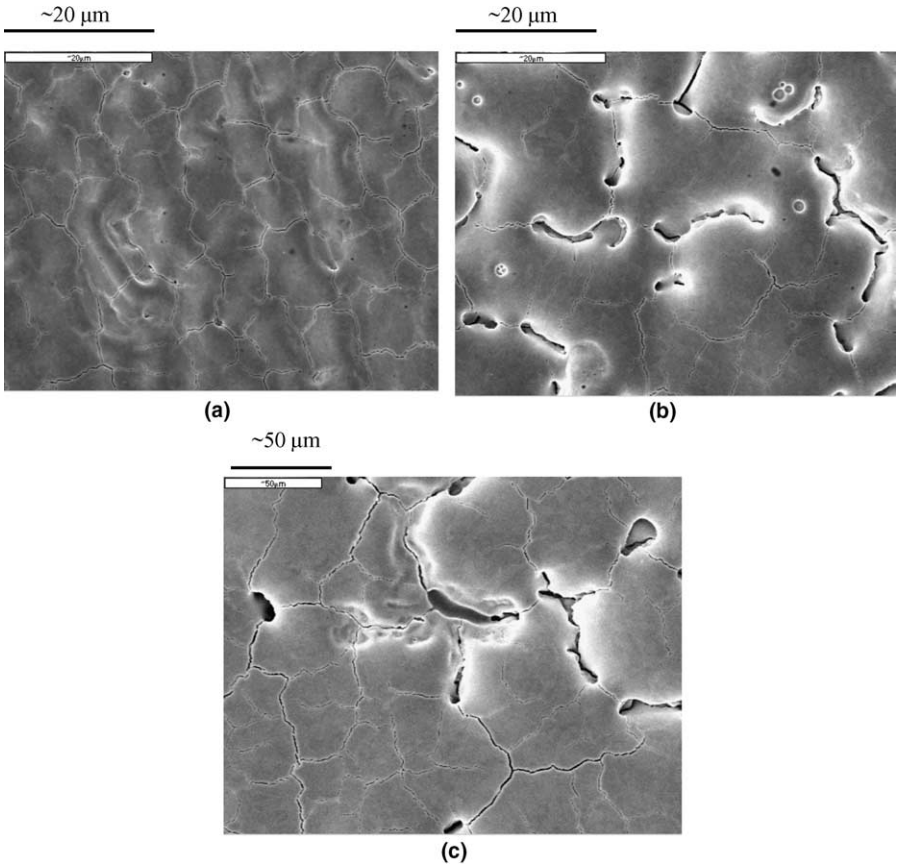

Fig. 13. SEM images of W25Re taken after 400 (a), 800 (b), and 1200 (c) nitrogen pulses. Fluence is approximately 1.7 J/cm^2.

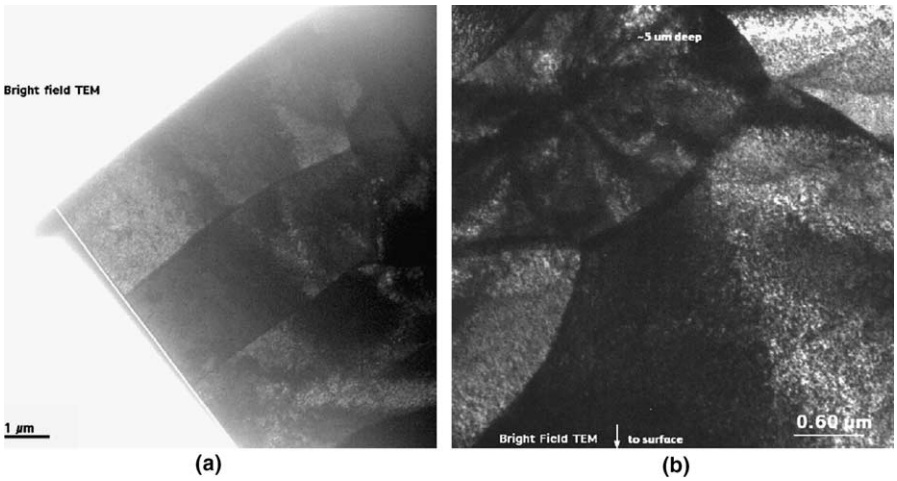

Fig. 14. Bright-field XTEM image: (a) PM W (heated to 600 °C) treated for 60 pulses at average fluence of 6 J/cm^2. This is approximately the ablation threshold. Note the epitaxial melt and recrystallization from a depth of almost 3 μm. (b) Same sample at 5 μm depth, showing no cracks or voids.

and relatively featureless, with an R_a value of about 0.4 μm. In depth (Fig. 14(b)), the appearance is that of the untreated W, i.e. large grains with no cracks or voids. Another PM W sample was exposed to 400

MAP N pulses at an average fluence of 7 J/cm^2. In this case, an ablation step of 20 μm was observed between treated and untreated portions. This amounts to an average of 50 nm of tungsten removed per pulse. However, the surface roughness R_a remained at about 0.5 μm, or much lower than in the cases discussed above of 2.5 and 4.5 J/cm^2 exposure. A nearby tungsten sample alloyed with 1% Lanthanum (W1%La) showed a 5 μm ablation step, with an R_a value of almost 2 μm and peak–valley excursion of 13.5 μm. The lower step is due to a slightly lower average fluence per pulse. The level of ablation is evidently very sensitive to the level of fluence above the nominal 6 J/cm^2 ablation threshold. Thus, the W1%La roughness is higher than the PM W exposed to 7 J/cm^2, but both surfaces are smoother than the PM W exposed to 2.5 and 4.5 J/cm^2. Interestingly, the PM Mo surface also exposed at about 6.5 J/cm^2 for 400 pulses showed the most dramatic surface topology. Periodically spaced peaks in the surface occur whose height exceeded the 80 μm measuring capability of the Dektak. It is estimated that the peak–valley excursion of the Mo is greater than 100 μm. In this case, then, the P Mo roughened worse than the PM W. However, the distinction is unimportant as a practical matter, since all of these samples suffered unacceptable levels of material loss at these fluences.

3.2. Other metals

The surface of the metals other than W and W25Re was periodically examined by SEM after a series of pulses. These other metals are Ti-2 (commercially pure), Re, and Mo, as well as Cu. These are not considered as leading contenders for armored wall surfaces, but their response is notable and will be discussed briefly. Re, in particular, is the only metal that does not have a brittle-ductile transition, and in fact work-hardens readily when commercially processed. So its materials response might be considered as more extreme even than W. Cu, on the other hand, is observed to develop little or no surface relief, even after 800 pulses that left the surface both below and above its melting point. This is presumably because of its malleability.

SEM examination of the metal surfaces indicates that each element (Cu excepted) develops its own pattern of surface relief. This is indicated by Fig. 15(a)–(d) and Fig. 16(a) and (b), which shows SEM images of Ti-2 and Re, respectively, as a function of fluence (MAP N beam). In all cases, the surfaces have been exposed to 1000 nitrogen beam pulses. Note that the surface of the treated Ti-2 exhibits a very complex appearance reminiscent of fractal patterning. The scale length of the surface deformation, i.e. the qualitative spacing between repeating features, appears to decrease with increasing fluence per pulse. This is not the case with Re, where the scale length increases with increasing fluence per pulse. In each image, the morphology appears to follow a distinct development path that is defined by the average fluence per pulse. The ultimate cause is probably connected with the set of bulk materials properties unique to each element. A complete model of such morphology evolution is beyond the scope of this paper, but such a model would be required to explain the qualitative feature differences seen in Figs. 15 and 16.

3.3. Carbon composite

We have previously reported [1] on the exposure of various forms of graphite to a mixed C/H ion beam. The materials response to this beam should be similar to that expected with the MAP N beam discussed above. The graphite forms were annealed pyrolytic graphite (PG), Poco (sintered graphite), and 4-d carbon-composite weave. The PG has a very high thermal conductivity in one direction, and its use in first walls would be oriented so that the high-conductivity direction is directed into the surface, so as to dissipate the most heat.

These forms of graphite were exposed to several series of beam pulses, up to 75 exposures per sample. Part of each sample was masked so that any step-height difference between unexposed and exposed surfaces formed by surface removal could be readily measured. The threshold of material ablation was observed to be between 2 and 3 J/cm^2, depending upon the graphite form. The Poco and composite matrix showed the lowest threshold, at about 2.5 J/cm^2, whereas the PG threshold was higher, at about 3.5 J/cm^2.

A BUCKY simulation of graphite was also performed, in which the PG properties were used. Using the MAP N beam characteristics, BUCKY predicts a threshold for surface removal at about 3.5 J/cm^2, which is consistent with that measured for the PG. Above this value, there occurs a rapid increase in the per-pulse ablation/sublimation rate as fluence is increased beyond this value. For example, at 4.5 J/cm^2, the rate of removal is predicted to be above 1/3 μm per pulse. This is clearly

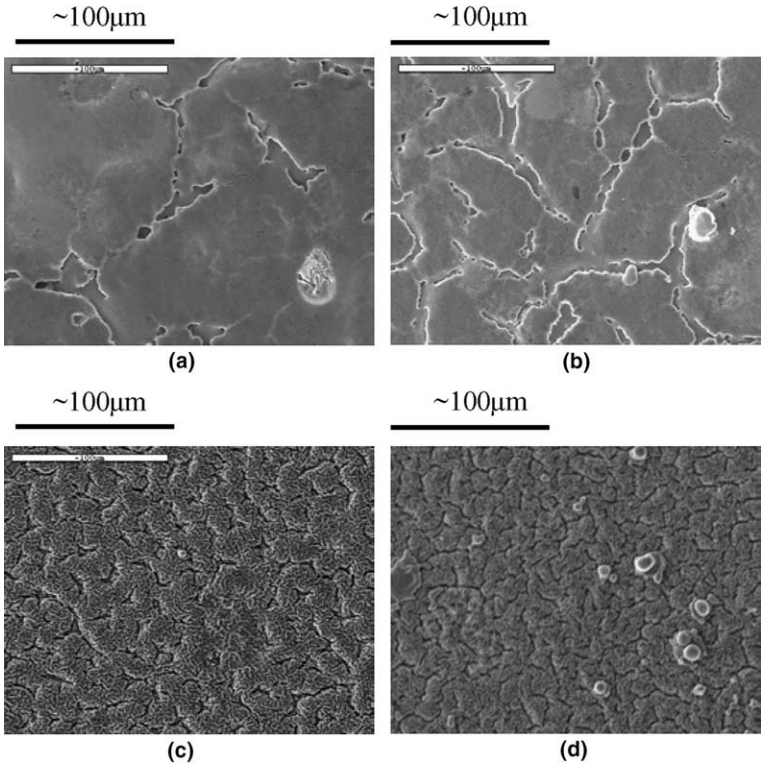

Fig. 15. SEM images of Ti-2 (commercially pure Ti) taken after 1000 pulses at an average of (a) 1.0 J/cm^2, (b) 1.6 J/cm^2, (c) 2.6 J/cm^2, and (d) 4.0 J/cm^2. Magnification is the same in all images.

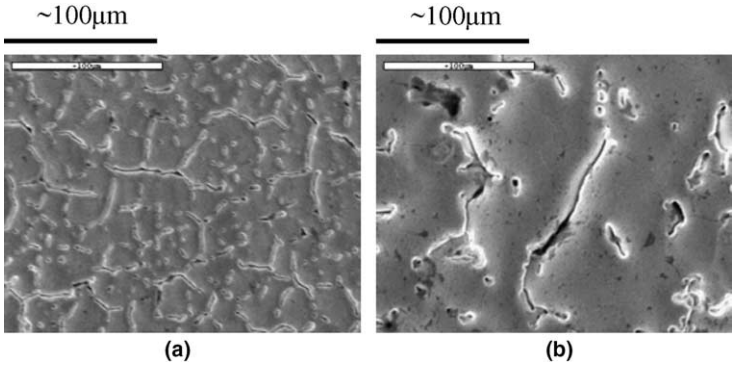

Fig. 16. SEM images of Re surface taken after 1000 pulses at an average of (a) 2.6 J/cm^2 and (b) 4.0 J/cm^2. Magnification is the same as in Fig. 15.

an unacceptable removal rate, and the sensitivity of the rate with fluence implies that the only option for wall use would be to restrict the wall fluence to below the 3.5 J/cm^2 figure.

The behavior of surface roughening with fluence varied more widely between Poco and PG. The Poco was observed to roughen at fluences below 1 J/cm^2. Surface roughness then increased strongly with fluence per pulse, up to as high as 3.5 μm at 4.8 J/cm^2 per pulse, over 75 pulses. Indeed, surface feature changes were observable at 0.5 J/cm^2 or even below. The PG, by contrast, did not develop surface roughening, even when the surface was ablated away.

The best overall study of graphite materials response is that of composites, which contain both ordered graphite (fibers), and sintered graphite (matrix) of no special properties. A study of the response of a particular composite, FMI-222, was undertaken, with samples surface-polished and exposed to 1000 pulses (MAP N) at 1.6 J/cm^2, and to 600 pulses each at 2.6 J/cm^2 and 4.0 J/cm^2. These values correspond to less than half the BUCKY ablation threshold (1000 pulses), and below and above the 3.5 J/cm^2 value from BUCKY (600 pulses), respectively.

A VEECO image of the FMI-222 treated at 1.6 J/cm^2 is shown in Fig. 17(a). The untreated area is on top, and treated at the bottom, with the interface located as a horizontal line about halfway between the image top and bottom. A linear R_a scan of the treated area appears in Fig. 17(b), and the same of the untreated area is shown in Fig. 17(c). Although the difference between treated and untreated areas is not readily apparent in the VEECO image, comparison of the two R_a scans shows that there is significant loss of material in the matrix between the fibers. The fibers appear as relatively flat areas in the scan shown in Fig. 17(b). Removal of material as deep as 60 μm below the surface is indicated. (The deep but narrow crevices indicated in the untreated area shown in Fig. 17(c) are due to surface preparation. Mechanical polishing separates the fibers from the matrix background, which produces the crevices.)

That this amount of material removal occurs at half the measured ablation threshold discussed above is significant. Further 1000 exposure series at lower fluence would help establish if there is an exposure fluence per pulse below which there is no matrix removal. But this level is expected to be well below 1.6 J/cm^2. Response at the higher fluences is shown in Fig. 18, at 2.6 J/cm^2 average per-pulse fluence (Fig. 18(a)), and at 4.0 J/cm^2 (Fig. 18(b)). A linear R_a scan of FMI-222 treated at 4.0 J/cm^2 is shown in Fig. 18(c). The scan is along the vertical line in Fig. 18(b), where the untreated area is towards the right, and interface is approximately in the middle. (The overall curvature from right to left is an artifact of the analysis.) A fiber is shown in the middle of the scan, after which the interface is reached, and there occurs a drop of 100 μm at the exposed matrix. Fig. 19 shows SEM images of untreated fiber (Fig. 19(a)), a fiber end treated at 4.0 J/cm^2 for 600 pulses (Fig. 19(b)), and treated matrix (Fig. 19(c)). All images are depicted at 500× magnification. The crevice caused by surface preparation is clearly evident in Fig. 19(a). The treated fiber end, which takes up most of the image shown in Fig. 19(b), shows a relatively benign response to the ion exposure. Note that the fiber end appears to be composed of a large number of smaller filaments. In contrast, the damage to the matrix material is quite evident. Images of treated matrix at the lower fluences also show damage, but in lesser amounts.

As discussed in Section 1, the pulsewidth here is shorter than that expected for a future reactor, so that the fluence levels indicated translate to higher allowed values in the latter case. Even so, at the anticipated 8–20 J/cm^2 in future reactors, it would appear that use of graphite in the first wall leads to an unacceptable loss of material.

3.4. 'Engineered' surfaces

The materials discussed above are of flat geometry. Thus, impinging ions will strike each point of the surface at maximum fluence. It may be the case that a more survivable surface might be possible if the surface is formed in some non-flat manner, e.g. a three-dimensional or 'engineered' surface. We discuss several versions of engineered surface below, the motivation for each, and results of ion exposure experiments with each.

(1) *Velvet*. In the discussion above of the FMI-222 carbon composite, it was pointed out that the carbon fibers survived ion exposure much better than did the carbon matrix. Two limiting forms of this material might then be considered. In one case, the matrix is replaced entirely by fibers. This may be hard to manufacture. In the other case, the matrix is removed, and only fibers remain. If then the fibers are arranged in long straight lengths, oriented along the direction towards the chamber center, this is referred to here as 'velvet'. The spacing between fibers can be varied. The impinging ion flux is presumed to have a non-zero transverse velocity component, even if very slight. Then while the fiber tips will receive the full force of the ion flux, the ions passing by the tips will impact the fiber sides at a glancing angle, and thus the effective fluence will be much reduced, compared to the fiber tips. The length and areal coverage of the fibers can be arranged so that little or no ion flux will penetrate to the substrate. If a surface coating can be applied that is thicker than the ion range expected from the fusion products, this could then act to protect the graphite from tritium buildup.

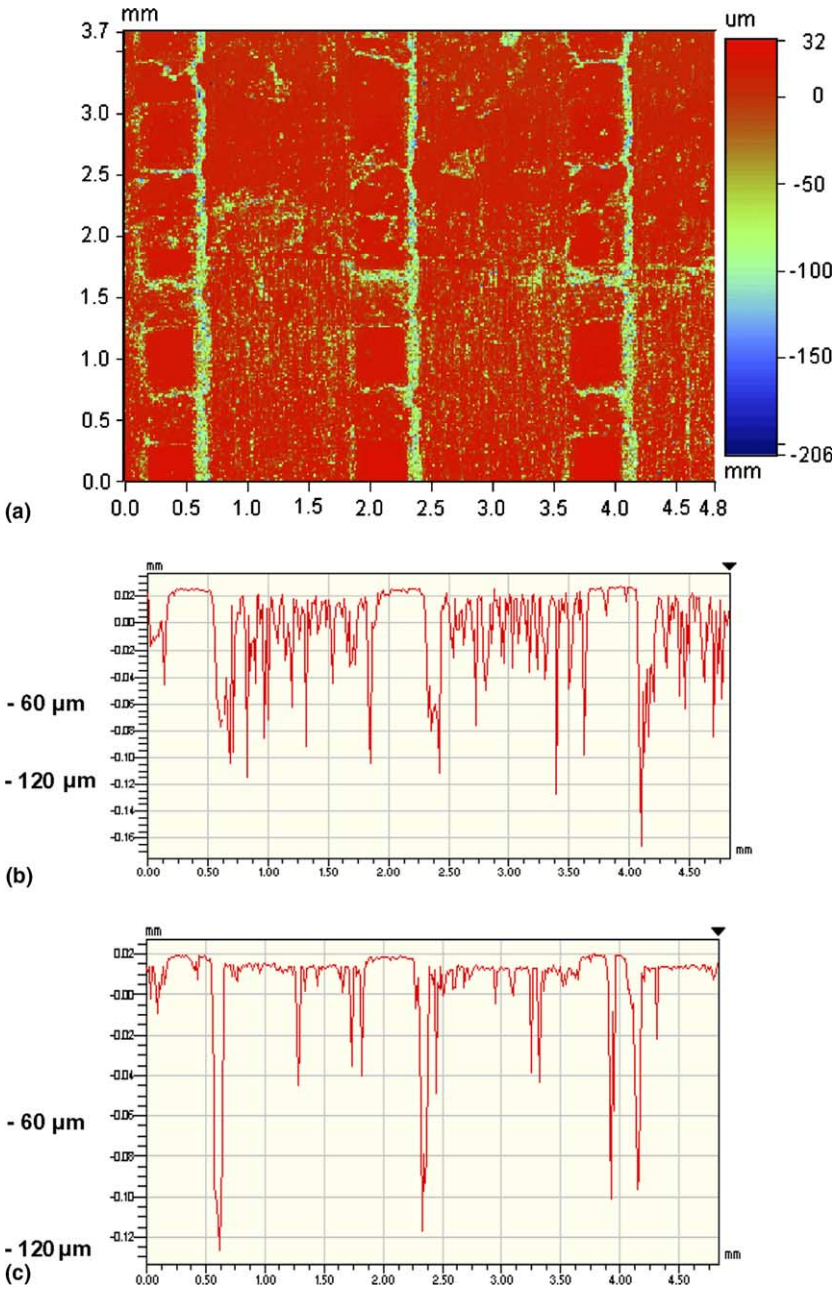

Fig. 17. (a) Two-dimensional VEECO image of FMI-222 CFC, treated with 1000 pulses (MAP N) at an average fluence of 1.6 J/cm^2. Untreated area occupies top half of image, treated the bottom half, with treatment interface a horizontal line approximately across the middle. Vertical crevices are an artifact of sample preparation. (b) Linear R_a scan across treated area. (c) Linear R_a scan across untreated area.

The first version of the 'velvet' that was exposed [1] consisted of a network of 2.5 mm-tall carbon fibers 6.5 μm in width, and attached to an aluminum substrate with epoxy adhesive. The packing fraction was 1.5%, i.e. only 1.5% of the substrate area had fibers connected. The qualitative results of this series of exposures was (1) removal of any fibers not oriented perpendicular to the incoming ions, (2) only slight damage to the fiber sides, and (3) physical removal of some fibers from the substrate, but in those areas where the fiber network remained in place, there was no damage to the Al substrate.

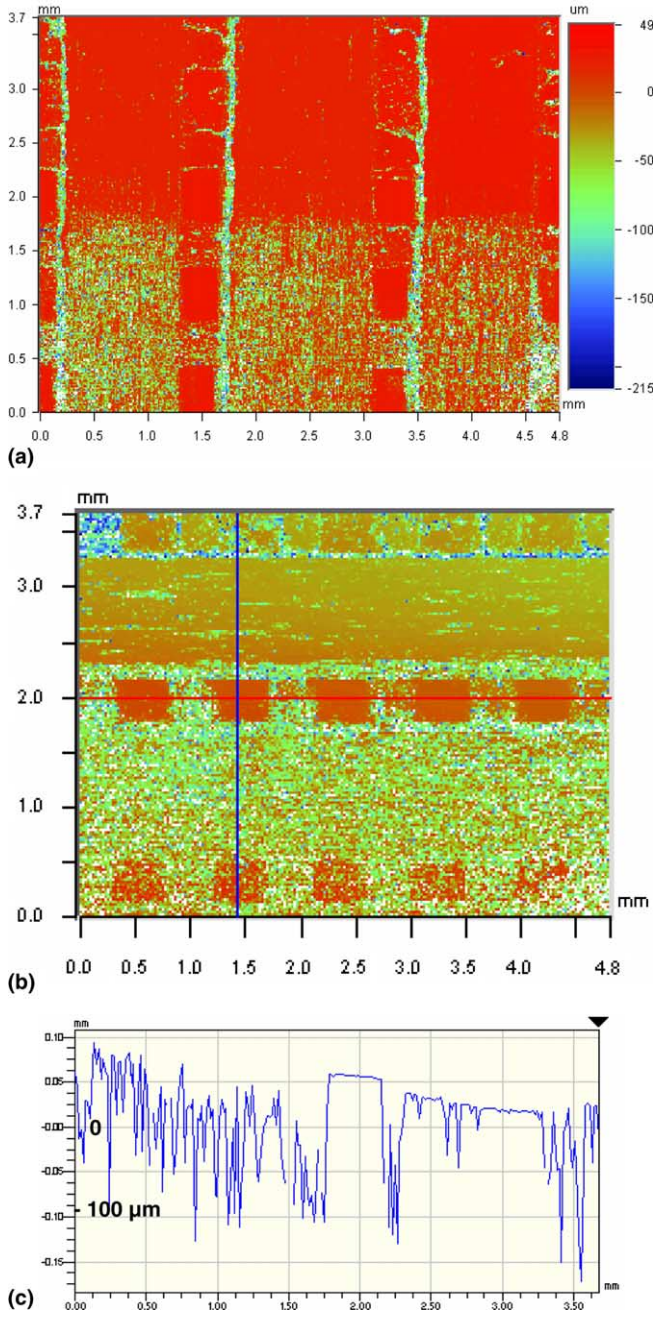

Fig. 18. Two-dimensional VEECO image of FMI-222 CFC, treated with 600 pulses (MAP N) at an average fluence of (a) 2.6 J/cm^2 and (b) 4.0 J/cm^2. Top half is untreated. (c) Linear R_a scan of FMI-222 treated at 4.0 J/cm^2. Scan is along the vertical line in (b), where the untreated area is towards the right, and interface is approximately in the middle.

The latter point is remarkable, since the epoxy adhesive is known to have a low melting point (approximately 100 °C).

The velvet version discussed here consists of a fiber network of packing fraction 1.9%, and attached to a graphite substrate. In addition, a 1.6 μm tungsten film was sputtered onto the fibers. The coating was thickest at the fiber tops, and less on the fiber side walls. The velvet was exposed to 200 pulses of the MAP N beam, at fluences ranging from 1 to 6 J/cm^2. The latter value is well above the carbon sublimation fluence, and roughly equal to

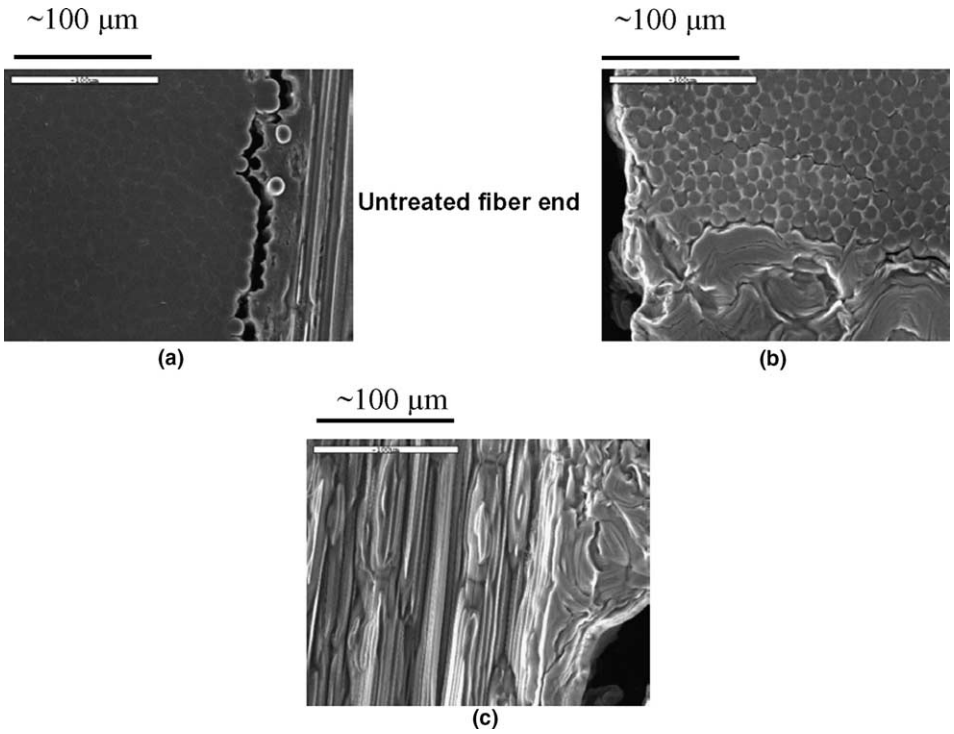

Fig. 19. (a) SEM image, FMI-222, showing fiber end, untreated. Magnification is 500×. (b) SEM image, FMI-222, fiber end exposed to 600 pulses, average 4.0 J/cm^2 per pulse. (c) SEM image, FMI-222, matrix exposed to 600 pulses, 4.0 J/cm^2 per pulse.

the W ablation threshold for the MAP N beam. After the treatment, the velvet was observed to be undamaged, even at the highest fluence. The substrate was also undamaged. The velvet was examined with SEM at the low, medium, and high parts of the 1–6 J/cm^2 range of fluences. The adhesion of the sputtered W to the fiber walls varied with fluence. At low fluence, there was extensive delamination of the W from the side walls, which then appeared as debris at the bottom of the fibers where they attach to the substrate. The delamination decreased significantly at the medium fluence level, and disappeared at the highest fluence, where no debris was observed at the substrate level.

The more interesting effect occurred at the fiber tips at the highest fluence. SEM images of two types of the tips are shown in Fig. 20(a) and (b). Most of the fibers consisted of tips which were flat. An example is shown in Fig. 20(a). The W on the tip has evidently melted and formed a ball (marked as #6 in the image). EDX analysis confirms this, and also confirms that the end and sides (marked #5 and #7) of the fibers contain only carbon. However, on about 10–15% of the fibers, the tip forms a point, on top of which the W was sputtered. In these cases (examples in Fig. 20(b)), the W has remained on the tip. Given that the coating was only 1.6 μm thick originally, the fact that this remains intact after 200 pulses of ablation-level fluence for W is remarkable. It may be possible to heat-treat the fibers to increase the adhesion between the carbon and tungsten, and also to sharpen all of the tips in order to retain the tungsten on top. Such a tungsten-coated carbon velvet may then become a viable engineered surface for long-term wall survivability.

(2) *Foam*. In the case of the W-coated velvet above, the apparently enhanced ability of the thin W coating to survive ion bombardment might be due to the non-bulk form of the tungsten. Another type of engineered surface consists of a lacework of 'bridges' surrounding imaginary spheres. An example of the geometry is shown in Fig. 21. The virtual spheres are about 1 mm in diameter. The principle is that in a three-dimensional structure, incoming ions would be stopped by one of the bridges before they penetrate to the substrate. In this form, the tungsten can be formed thinly enough so that entrained He from the fusion events may be able to diffuse to the surface of the bridges, so as to avoid He bubble formation. In addition, the

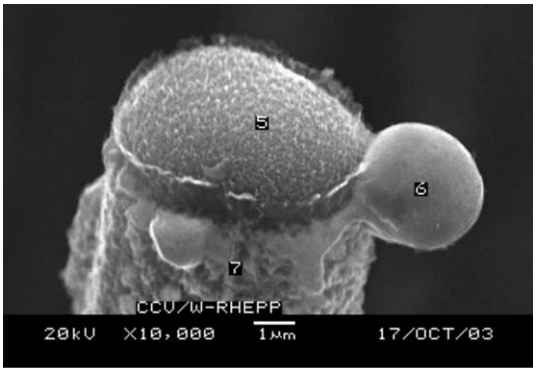

(a)

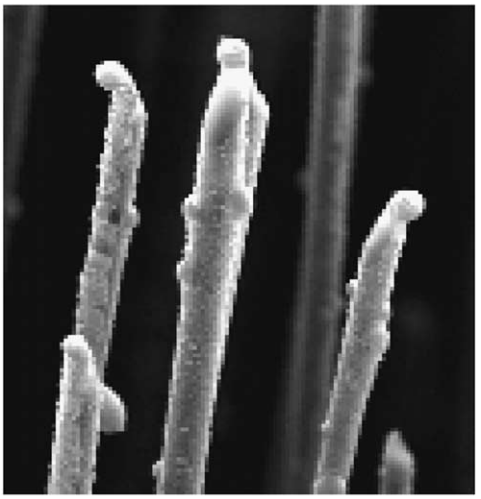

(b)

Fig. 20. (a) SEM image, 'velvet' fiber tip, flat geometry. EDX of top and sides showed carbon composition (5 and 7), and tungsten has formed a ball on the fiber side (6). (b) SEM image, 'velvet' fiber tip, tapered tip. The 1.6 μm W coating remains in place.

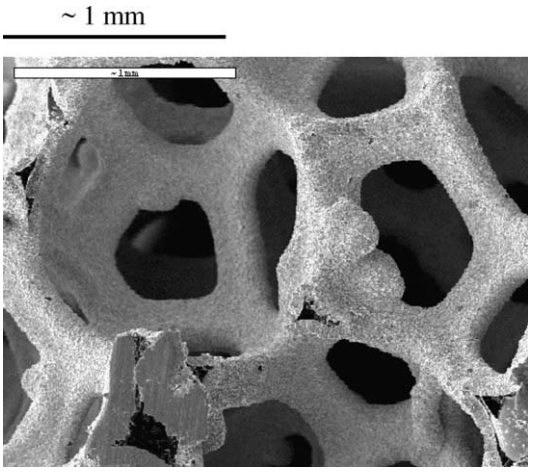

Fig. 21. SEM image, 'Foam' geometry. Magnification 50×.

tungsten in this form may prove superior in ductility and other properties to the polycrystalline bulk form studied in Section 3.1 above. Then the network aspect ratio and bridge width can in principle be adjusted to optimize performance. It is presently not known how small in width the bridges must be to allowed for He to diffuse out, but it is generally recognized that the bridge structure indicated in Fig. 21 is too large.

Two versions of this Foam were treated by up to 1600 pulses of nitrogen ions. The Foams were heated to 600 °C during these exposures. Both were made from an initial bridgework of graphite, over which either TaC or HfC was formed, followed by

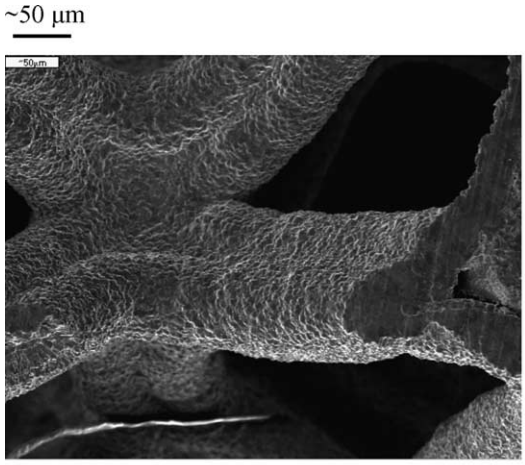

(a)

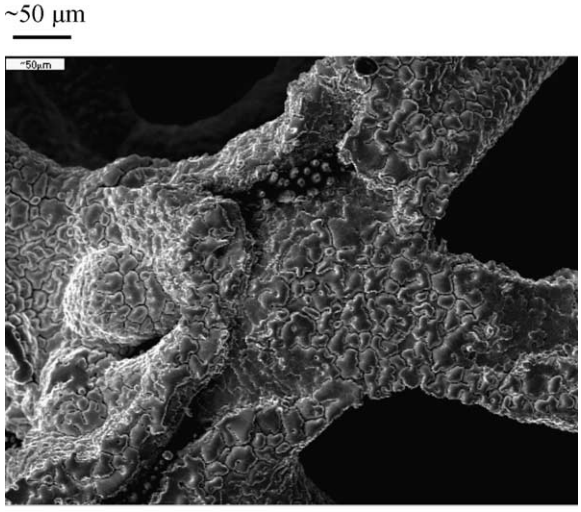

(b)

Fig. 22. SEM image, W-coated TaC Foam, untreated (a) and after 1600 pulses at an average fluence of 1.5 J/cm^2 (b). Both images at 250× magnification.

tungsten deposited by CVD. The graphite was then removed by heat-treatment. The W thickness was 30 μm in the case of the TaC substrate, and 15 μm for the HfC. The W/TaC surface was subjected to an average fluence of 1.5 J/cm^2 over the pulses, with the fluence varying between 1.2 and 1.7 J/cm^2. SIM heat-flow modeling predicts a peak surface temperature between 2730 and 3550 K, i.e. the W surface is not predicted to melt. The W/HaC, exposed to a lower fluence portion of the beam, experienced a lower variation in fluence, from 0.5 to 1.2 J/cm^2 (1670–2880 K). After each set of 400 pulses, the Foams were demounted and the surface analyzed with SEM, until all 1600 pulses were taken. The images then are of different but representative areas of the W/TaC and W/HfC surface.

Fig. 22 shows SEM images (250× magnification) of the W/TaC surface, both untreated (Fig. 22(a)) and after 1600 pulses (Fig. 22(b)). The untreated surface appears wrinkled and with some suggestion of grooves, but no cracks or breaks. After 1600 pulses, a complex network of cracks is observed to form. The evolution of morphology of these cracks can be seen in the SEM images shown in Fig. 23, which show closeups (2500× magnification) of various areas after 400 (a), 800 (b), 1200 (c), and 1600 (d) pulses. The initial cracks appear to widen with number of pulses, and new cracks then appear in the flat spaces between the cracks. The widening is evidently erosional, so that over time, mass loss could be significant.

While erosional material loss appears to happen with the W/TaC, in the W/HfC, the process resembles more brittle destruction. This can be seen by comparing the SEM images in Fig. 24, which show the untreated surface (a), and after 800 pulses (b), both at 250× magnification. In Fig. 24(b), the top half of the W/HfC bridge structure has blown off, exposing the backside. Evidence of the absence of crack erosion is shown in Fig. 25. Comparison of the high-magnification (7500×) images of the W/HfC surface (a) and W/TaC surface (b)

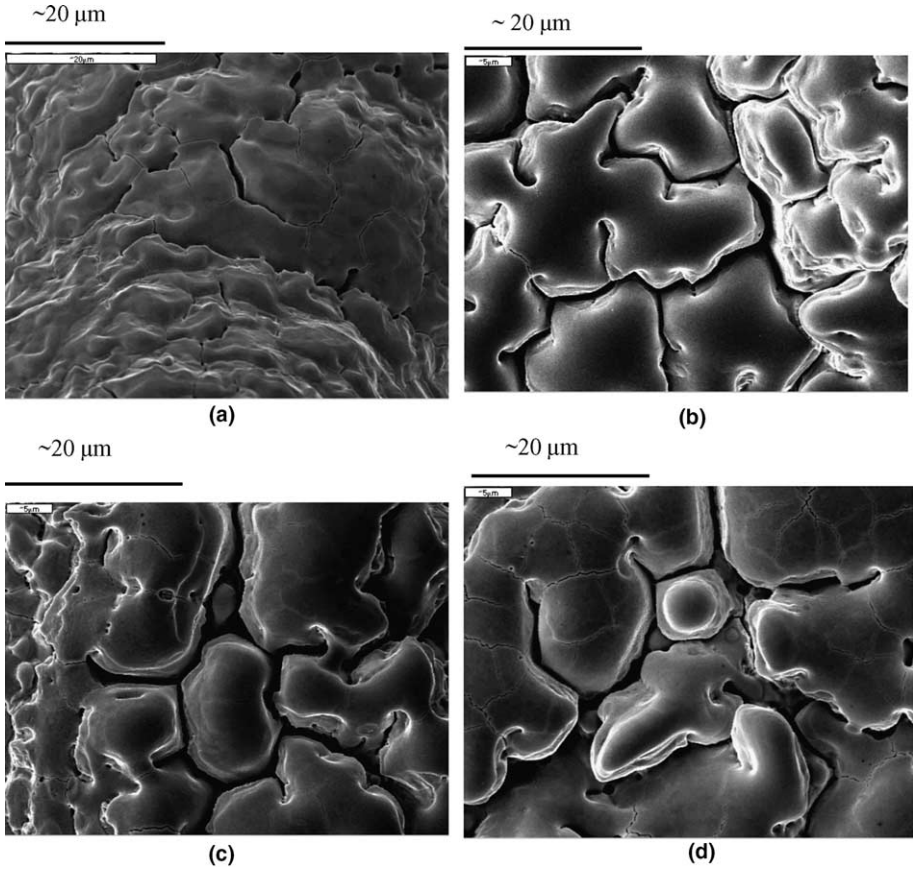

Fig. 23. SEM images, W-coated TaC Foam, after (a) 400, (b) 800, (c) 1200, and (d) pulses. Magnification is 2500×. Images are of different areas on Foam surface.

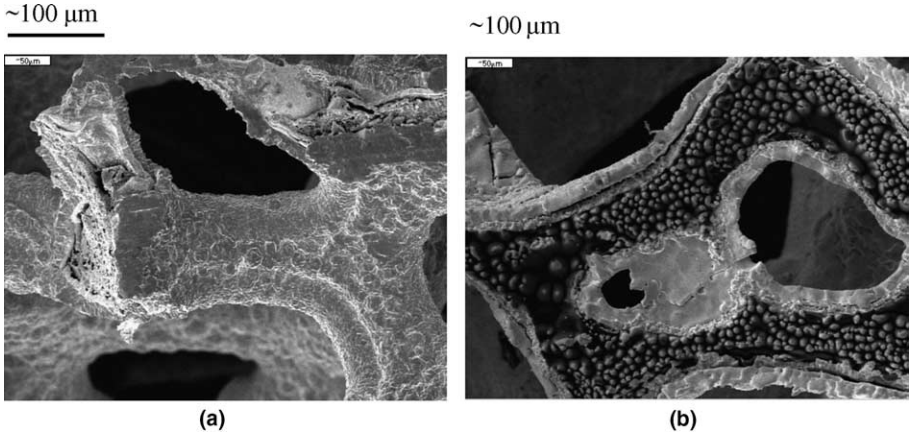

Fig. 24. SEM images, W-coated HfC Foam, untreated (a) and after 800 pulses (b). Magnification is 250×.

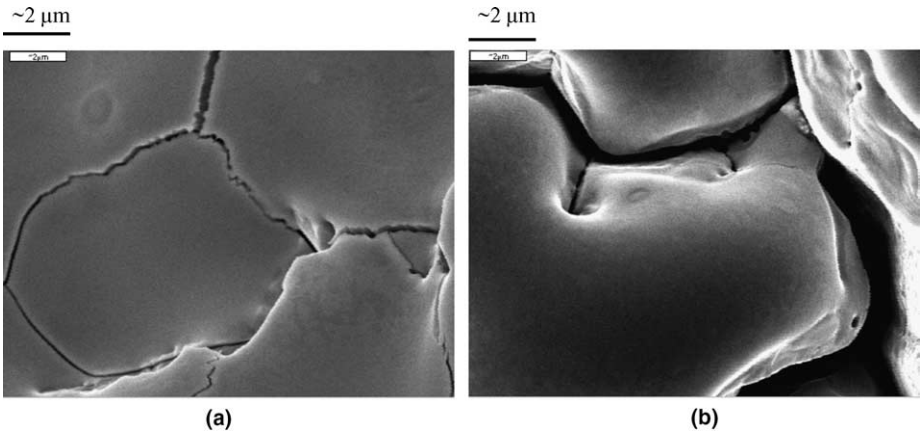

Fig. 25. SEM images, W/HfC (a) and (b) W/TaC Foams exposed to 800 pulses. Magnification is 7500×.

indicate the lack of crack widening on the W/HfC surface.

Both of these W/TaC and W/HfC surfaces are thus seen to suffer failure. The mechanisms are different in the two case. The reasons for this are unclear, but may have to do with the difference in thickness of the W coating in the two cases, or the adhesion of the W to the respective substrates, or differences in bulk behavior of the substrates. But it appears that, particularly in the case of the W/TaC, the thin W coating appears to suffer surface roughening and crack formation similar to that seen on the surface of the (flat) bulk W samples.

4. Discussion

Were it not for the cracking and formation of voids seen with the PM W after ion exposure, the surface roughening also seen by itself might be tolerable as a surface response, since the actual loss of surface material has not been confirmed. The response of the tungsten when heated to 600 °C also appears to be more benign than if the surface is left unheated, although both surfaces roughen worse than all the other samples investigated. The only exception was when W and Mo were both subjected to fluences above their ablation thresholds. Then the surfaces were rendered much smoother, but of course at this point, unacceptable amounts of material loss occurred.

The carbon composite material demonstrates a weakness of carbon as seen in previous measurements. Above the sublimation point, there is a rapid increase in the material removal rate. With the matrix material, there is loss well below the measured and modeled sublimation point. Perhaps

physical sputtering or radiation-enhanced sublimation is the cause. The carbon velvet performed quite well. However, the graphite fiber cores are expected to suffer significantly under the neutron bombardment that will occur in future reactors. Both forms of foam tested suffer mechanical failures. The indication is that, at least for the kind of foam structure investigated here, the W contained in the foam behaves similarly with bulk PM tungsten.

The effects of helium absorption and bubble formation have not been studied in this investigation. The 450-pulse series with He is estimated to have introduced 4.5×10–15 atoms/cm^2 into the surface (at the rate of a monolayer of atoms per pulse). This is below the level of implantation required to observe He bubble formation as reported by most researchers. Other than the enhanced surface roughening produced compared with nitrogen beams of the same fluence, no other effects of He beam use have been discovered.

5. Summary

Candidate materials for the first wall of a future IFE reactor have been investigated using pulsed intense ion beams generated by the RHEPP-1 facility at Sandia National Laboratories. Materials in flat geometry include pure tungsten in powder metallurgy (PM) polycrystalline form, and also CVD and single-crystal forms. Tungsten alloyed with 25% rhenium (W25Re) was also investigated. Other metals exposed include Molybdenum, commercially pure Titanium, and pure Rhenium. 'Engineered materials' were also investigated – a 'velvet' consisting of carbon fibers over which a 1.6 μm layer of tungsten was sputtered, and two kinds of 'Foam', each with a CVD coating of tungsten over either a TaC or HfC substrate in a 'bridge' structure.

The surface of the PM W is observed to undergo surface roughening below the level of exposure needed to cause surface melting. This roughening has a relatively low threshold, about 1.25 J/cm^2 at these pulsewidths. Above this threshold, the surface is observed to undergo progressive roughening over the course of up to 1600 pulses. The roughening scales with the fluence, and with the number of pulses, but appears to reach a plateau. The level of roughening can reach very high levels, with surface R_a up to 20 μm, and peak–valley excursions of 70 μm. The surface height of the treated W increases compared to an untreated surface. Cracks and voids are seen in both horizontal and vertical directions of treated but unmelted surfaces, down to at least 10 μm depths. Evidence of deeper crack formation will be discussed in a future publication. Similar exposures of W25Re alloy result in much less surface roughening, and no evidence of the horizontal striations seen with the PM W. In addition, the CVD and single-crystal forms of tungsten were observed to roughen considerably less than the PM W. The latter were only exposed to a 450-pulses series using a He beam. All the other treatment series discussed were made with a nitrogen beam. The He beam also produced more roughening than the nitrogen beam, for the same fluence.

The mechanism for this roughening and cracking appears to be thermomechanical in nature, and connected directly with the pulsed thermal energy delivery. The near-surface expands in response to the rapid heating, and the subsequent cool-down leaves the region in tension. This is indicated anecdotally by the curling of thin samples after exposure. The reason for the more severe roughening of the PM W compared to the CVD and single-crystal W forms is not clear. There is evidence from both experimental data and response modeling studies that each grain can develop a topology different from neighboring grains, and that the summation of all these responses can lead to the roughening seen. The reason for the treated height being raised relative to the untreated level ('mountains') may be simply the CTE expansion of the heated tungsten. The relative poor showing of PM tungsten has implications for Magnetic Fusion Energy (MFE) wall materials as well as IFE, since Edge-Localized Mode (ELM) discharges are expected to occur at ~1 Hz in future tokomaks. The cycle time is longer than the 100 ns period seen for ion deposition in IFE, but tungsten can be expected to develop a fatigue response in time.

The carbon 'velvet' appeared to survive a 200-pulse exposure well, whereas the foams both experienced failures, but for different reasons. The W/TaC surface evolved into a series of cracks, the widths of which appeared to widen with further exposures. The W/HfC surface did not experience crack widening, but instead suffered brittle failures. This is evidently due to the brittle nature of HfC. In either case, the use of relatively thin tungsten layers in the foam seems not to have mitigated its deleterious bulk properties.

It appears that some modification must be made to conventional PM tungsten, to allow its use in a

pulsed reactor environment. Investigation of the anticipated preferred form of tungsten for the Laser IFE first wall, i.e. a PVD W layer on top of ferritic steel, will be undertaken after this material is successfully synthesized. Alloying with Re appears to produce more desirable surface properties. Some form of engineered (e.g. non-flat) surface may also ultimately prove successful in surviving the periodic energy flux from a fusion reactor.

Acknowledgement

Gerard Torres provided able technical support for the experimental activities on RHEPP-1.

References

[1] T.J. Renk, C.L. Olson, T.J. Tanaka, M.A. Ulrickson, G.A. Rochau, R.R. Peterson, I.E. Golovkin, M.O. Thompson, T.R. Knowles, A.R. Raffray, M.S. Tillack, Fus. Eng. Des. 65 (2003) 399.

[2] R.R. Peterson et al., Fus. Technol. 30 (1996) 783; R.R. Peterson, D.A. Haynes Jr., I.E. Golovkin, G.A. Moses, Phys. Plasmas 9 (2002) 2287.

[3] M.O. Thompson, T.J. Renk, Mater. Res. Soc. Symp. Proc. 504 (1998) 33.

[4] T.J. Renk, T.J. Tanaka, C.L. Olson, R.R. Peterson, T.R. Knowles, J. Nucl. Mater. 329–333 (2004) 726.

[5] Foam provided by Ultramet, Pacoima, CA.

[6] Tina Tanaka, private communication.

[7] J.P. Biersack. J.F. Ziegler, Transport of Ions in Matter, IBM Research, Yorktown Heights, NY, 1995.

[8] T.J. Renk, P.P. Provencio, S.V. Prasad, A.S. Shlapakovski, A.V. Petrov, K. Yatsui, W. Jiang, H. Suematsu, Proc. IEEE 92 (2004) 1057.

[9] H.C. Harjes, K.J. Penn, K.W. Reed, C.R. McClenahan, G.E. Laderach, R.W. Wavrik, J.L. Adcock, M.E. Butler, G.A. Mann, G.E. Pena, G.J. Weber, D. VanDeValde, L.E. Martinez, D. Muirhead, P.D. Kiekel, D.L. Johnson, E.L. Neau, Initial Results from the RHEPP module, in: D. Mosher, G. Cooperstein (Eds.), 9th International Conference on High-Power Particle Beams (Beams 92), Washington, DC, NTIS PB92-206168, p. 333.

[10] ITER Materials Properties Handbook. Available from: <http://www-ferp.ucsd.edu/LIB/PROPS/ITER/>.